Polymer enrichment decelerates surfactant membranes near interfaces

F. Lipfert,[1] H. Frielinghaus,[2] O. Holderer,[2] S. Mattauch,[2] M. Monkenbusch,[1] N. Arend,[2,3] and D. Richter[2,1]

[1]*Institute for Complex Systems 1, Forschungszentrum Jülich GmbH, D-52425 Jülich*

[2]*Jülich Centre for Neutron Science at Heinz Maier-Leibnitz Zentrum, Forschungszentrum Jülich GmbH, Lichtenbergstr. 1, D-85747 Garching*

[3]*Jülich Centre for Neutron Science (JCNS), Outstation at SNS, Oak Ridge, USA*

(Received 23 October 2013; published 14 April 2014)

Close to a planar surface, lamellar structures are imposed upon otherwise bulk bicontinuous microemulsions. Thermally induced membrane undulations are modified by the presence of the rigid interface. While it has been shown that a pure membrane's dynamics are accelerated close to the interface, we observed nearly unchanged relaxation rates for membranes spiked with large amphiphilic diblock copolymers. An increase of the polymer concentration by a factor of 2–3 for the first and second surfactant membrane layers was observed. We interpret the reduced relaxation times as the result of an interplay between the bending rigidity and the characteristic distance of the first surfactant membrane to the rigid interface, which causes the hydrodynamic and steric interface effects described in Seifert's theory. The influence of these effects on decorated membranes yields a reduction of the frequencies and an amplification of the amplitudes of long-wavelength undulations, which are in accordance to our experimental findings.

DOI: 10.1103/PhysRevE.89.042303 PACS number(s): 82.70.Kj, 68.03.Kn, 68.08.De, 87.16.dj

Surfactant systems have a wide range of applications in surface cleaning, especially when classical effluent solvents are replaced [1]. Soil cleaning involves huge surfaces from which the contamination needs to be removed [2]. Microemulsions often appear in these applications, arising directly from the formulation or from the contact of aqueous surfactant systems with oily substances [3]. At this point, additives that allow the reduction of the expensive surfactant amount will make the aqueous surfactant system cost effective. Apart from static studies, realistic situations involve flow fields that are quite well understood on macroscopic length scales, while the microscopic effects demand a better understanding [4,5]. One first attempt at describing the effective boundary conditions is the introduction of a slip length [6] that might even dominate the behavior in small pores [7]. But this approach might not describe all possible aspects and, therefore, detailed studies of surface effects (structure and dynamics) of complex fluids are needed.

The first microscopic characterizations of three-component microemulsions near planar surfaces have been carried out in terms of analyzing structure [8] and dynamics [9,10]. Microemulsions consist of water and oil and the mediating surfactant, which leads to macroscopically homogenous fluids. Microscopically, there are domains of pure water and oil with typical sizes of 10 nm, and the surfactant covers the interface between the domains. Close to the surface, the structure becomes lamellar with similar domain sizes. There, dynamics that are about three times faster are observed by grazing-incidence neutron spin-echo spectroscopy (GINSES). The challenge of this new technique is that the low intensities stemming from the small volume of thin layers near the surface must still allow reasonable statistics to be obtained. The experimental findings could be addressed to the well-known lubrication effect. The parallel lamellae allow facilitated slipping of the fluid, and this coincides with the faster dynamics. For microemulsions, the theoretical concept was elaborated by Seifert, and the neutron spin-echo (NSE) relaxation curves were described by transferring the new dispersion relation to the classical Zilman-Granek theory (elaborated in [9]). The new concept includes reflections of hydrodynamic waves between the first membrane and the solid surface.

Amphiphilic polymers proved to be the most interesting additives in microemulsions [11–14]. For instance, the polymer boosting effect describes the dramatic increase of surfactant efficiency for microemulsions with polymer-decorated surfactant membranes. The conformational polymer entropy exerts a pressure on the fluctuating membrane and thus leads to membrane stiffening and flattening. This in turn allows for larger domains with a better surface to volume ratio, which explains the higher surfactant efficiency. A more general survey about polymer additives is given in Refs. [15,16]. Polymer additives in microemulsions in contact with solid surfaces are an interesting topic giving rise to questions about structure, dynamics, and functionality.

In the current study we investigated the effect of symmetric amphiphilic diblock copolymers on the near-surface membrane dynamics. A first step in investigating these polymers will focus on surface effects. The polymer distribution and the lamellar ordering are studied by grazing-incidence small-angle neutron scattering (GISANS), while the dynamics are studied by GINSES. We briefly summarize the theoretical concepts and then directly present the results.

The microemulsion structure has been investigated with GISANS at the magnetic reflectometer with high incident angle (MARIA) at the FRM-II research reactor. Dynamics have been studied using GINSES at the J-NSE instrument (FRM-II) [17,18] and at the SNS-NSE at the Spallation Neutron Source in Oak Ridge [19]. In grazing-incidence methods like GISANS and GINSES, the sample is illuminated by an evanescent neutron wave through the flat surface of a hydrophilic Si block. The scattering depth of the evanescent wave can be varied by changing the incident angle α_{in} or by changing the contrast $\Delta\rho$ between Si and the microemulsion with different degrees of deuteration. The evanescent wave decays exponentially with the scattering depth $\Lambda = \Lambda_{in} = [4\pi\,\Delta\rho(1 - \alpha_{in}^2/\alpha_c^2)]^{-1/2}$ [assuming the exit angles are high,

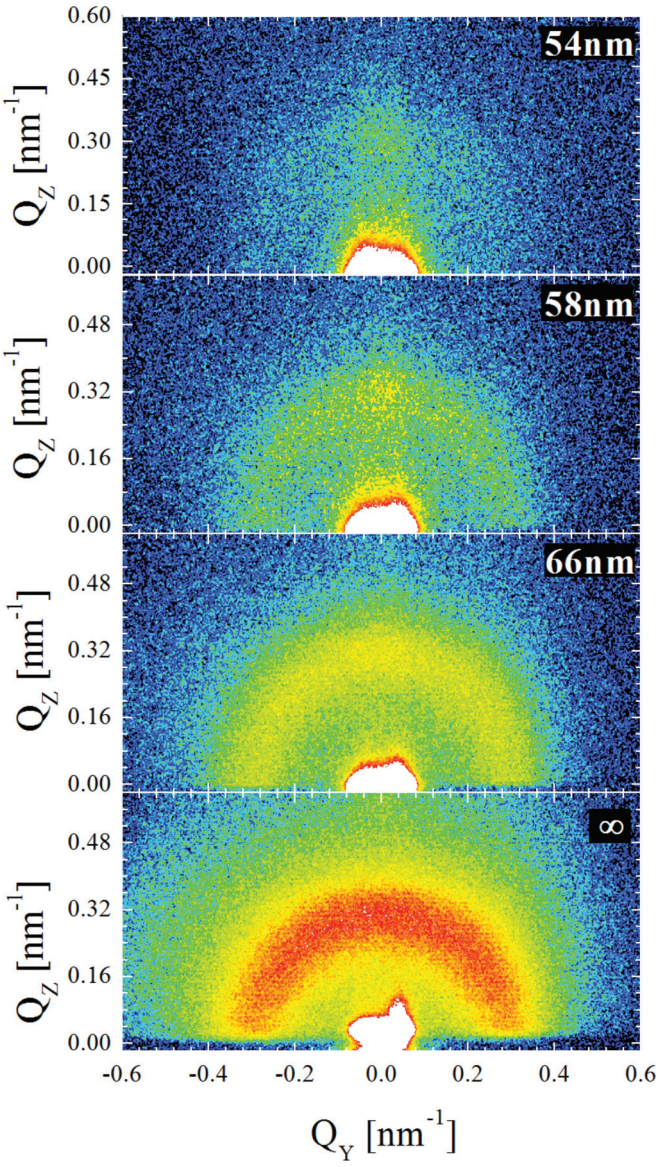

FIG. 1. (Color) GISANS intensities for different incident angles leading to different scattering depths Λ. For $\Lambda = 54$ nm, the lamellar peak at $(Q_y, Q_z) = (0,0.32)$ nm^{-1} starts to be well distinguished from the background. For $\Lambda = 58$ nm, the isotropic contribution appears weakly at $|Q| = 0.32$ nm^{-1}. Finally, at $\Lambda = 66$ nm the bicontinuous bulk structure prevails.

and no damping occurs during the exit, i.e., $\Lambda_f = \infty$, and $\Lambda = (\Lambda_{in}^{-1} + \Lambda_f^{-1})^{-1}$]. Structural and dynamic information can thus be gathered from highlighted regions with different extents into the microemulsion sample.

Bicontinuous microemulsions consisting of water and decane and the nonionic surfactant $C_{10}E_4$ with the same concentrations as in Refs. [8–10] were used. For the structural analysis, we used a sample consisting of 41.5% D_2O and 41.5% $C_{10}H_{22}$ (volume fractions). The amphiphile fraction of 16.9% was made of 98% $C_{10}E_4$ and 2% polymer. The amphiphilic diblock copolymer consisted of polyethylene propylene (PEP) and polyethylene oxide (PEO), with a molecular weight of 5 kg/mol per block. The measurements were performed with a wavelength of 1 nm, which leads to a critical angle of total reflection of $\alpha_c = 0.20^\circ$ and a minimal scattering depth of $\Lambda_{min} = (4\pi\,\Delta\rho)^{-1/2} = 45$ nm. For the GINSES experiments, the sample contained 36.5% $C_{10}H_{22}$ and 5.0% $C_{10}D_{22}$. The GINSES experiments were performed with a wavelength of 0.8 nm, which yields a critical angle of $\alpha_c = 0.22^\circ$ and a minimal scattering depth of $\Lambda_{min} = 32.5$ nm.

Figure 1 illustrates the structural results, giving insight into the near-surface structure, which is very similar to the sample without the polymer, investigated in [8]. For small scattering depths, the preferred parallel orientation of the lamellar region is visible from the correlation peak at $(Q_y, Q_z) = (0,0.32)$ nm^{-1}. The isotropy of the bicontinuous phase leads to a scattering on Debye-Scherrer rings with radius $|Q| = 0.32$ nm^{-1}, which indicates identical repeat units (ca. 20 nm) or single domain sizes (ca. 10 nm) in either structure. For the structural analysis, we used the same fit function as presented in [8] to obtain the characteristic intensity ratio of the two scattering contributions I_{bic} and I_{lam}. The idea behind that function is the Laplace transformation of step functions describing the regions of the lamellar and bicontinuous regions, i.e., $I_{bic} \sim \int_Z^\infty \exp(-2z/\Lambda)dz$ and $I_{lam} \sim \int_0^Z \exp(-2z/\Lambda)dz$ for a sharp boundary at depth Z and independent, uncorrelated scattering volumes (which is true for the bicontinuous microemulsion with the correlation length $\xi \sim 10$ nm $< Z \sim 40$–50 nm). Empirically, the reduction of this ratio to the asymptotic behavior describes the experiments better, i.e.,

$$\frac{I_{bic}}{I_{lam}} = \begin{cases} 0 & \text{for } \Lambda < Z, \\ S(\Lambda - Z) & \text{for } \Lambda > Z. \end{cases} \quad (1)$$

The slope S describes the intensity ratio of a bicontinuous versus a lamellar microemulsion. For low scattering depths, the bicontinuous intensity is negligible because the microemulsion is purely lamellar near the surface. For larger scattering depths, the contribution of I_{bic} increases linearly while I_{lam} stays constant due to the full illumination close to the surface. The depth of the bicontinuous phase is determined to be $Z = 53$ nm, from the extrapolation of the ratio I_{bic}/I_{lam} to zero (Fig. 2).

Parallel GISANS measurements focused on the diffuse scattering of the membrane and the polymer (compared to the pure microemulsion) by using protonated surfactant and polymer but deuterated water and oil (film contrast condition). The diffuse scattering intensities were weakly structured and

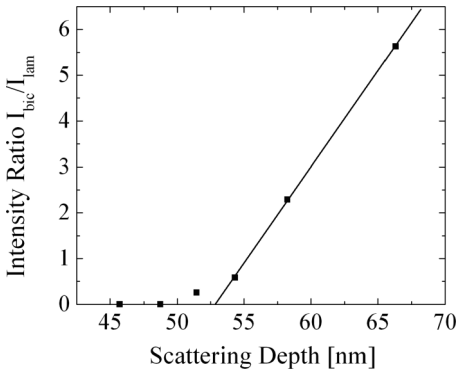

FIG. 2. Intensity ratio of the bicontinuous and lamellar signals in a GISANS experiment on the microemulsion with polymer additive.

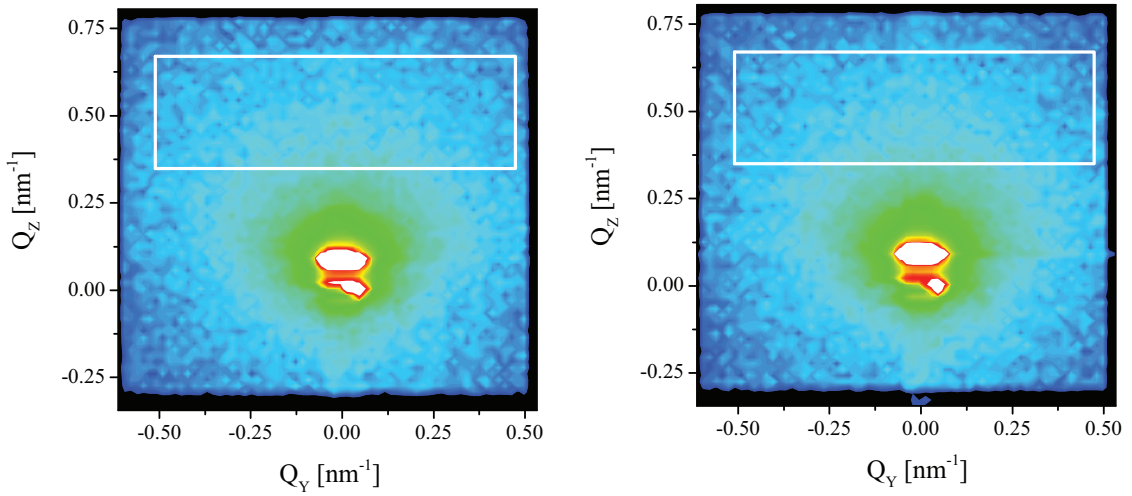

FIG. 3. (Color) Intensity plots of film contrast GISANS measurements with logarithmic color scaling. The scattering depth was $\Lambda = 21$ nm. The passing primary beam and the specular reflex are colored white due to the high intensities. The right graph was taken for the same conditions with polymer added. The white boxes indicate the range of intensity integration used to obtain the excess polymer scattering.

weak in terms of intensity (Fig. 3). By simple integration over the (Q_y, Q_z) plane (± 0.5 nm^{-1}, 0.37–0.65 nm^{-1}), we obtained an intensity-depth dependence that is proportional to the total amphiphile concentration. The excess polymer scattering $I_{\text{pol}}/I_{\text{surfactant}}$, normalized by the pure surfactant scattering, is depicted in Fig. 4. Polymer enrichment is clearly visible for a zone of 17 ± 1 nm near the solid surface. The solid line of Fig. 4 arises from an interpolation between two polymer concentrations ϕ_{surface} and ϕ_{bulk} according to

$$\frac{I_{\text{pol}}}{I_{\text{surfactant}}} = \frac{\phi_{\text{surface}}}{1+R} + \frac{\phi_{\text{bulk}}}{1+R^{-1}}. \qquad (2)$$

The ratio R arises from an intensity ratio similar to Eq. (1), but with the boundary $Z = 17 \pm 1$ nm for two lamellae with higher polymer concentration and a particularly fitted amplitude S.

A thermally fluctuating membrane in a viscous medium can be described with the Zilman-Granek model [20]. The dispersion relation of the membrane fluctuations $\omega(k) = \kappa k^3/(4\eta)$ is proportional to the third power of the undulation wave vector k. The viscosity here is denoted with η and the bending rigidity with κ. According to the theory of Seifert [21,22] a rigid interface close to the undulating membrane changes this dispersion relation to a k^2 dependence for long-wavelength undulations (Fig. 5). The transition between the short-range k^3 dependence and the long-range k^2 dependence takes place at a characteristic wave vector $k \sim \bar{l}^{-1}$, the reciprocal distance of the first membrane from the rigid interface. The cut off wavelength $k_{\text{min}} \propto 1/\xi$ of the undulation modes is limited by the persistence length ξ, which describes the size of nearly planar patches forming the whole membrane. At the interface, it is plausible that ξ is practically infinity, while in the bulk the persistence length is set equal to the reciprocal width

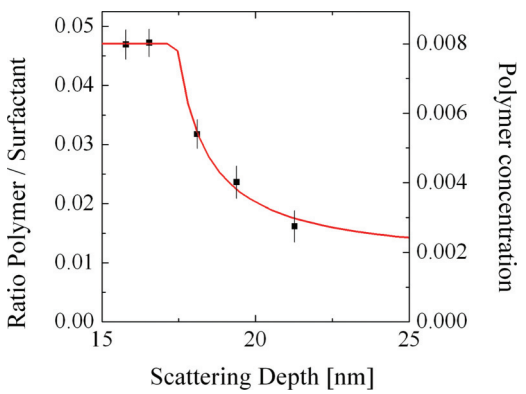

FIG. 4. (Color online) Excess polymer, diffuse GISANS intensities. The solid line interpolates the near-surface and bulk concentration with a sharp near-surface layer of 17 ± 1 nm. Deep in the bulk, the initial polymer weight is reached, while the near-surface concentration is about three times higher.

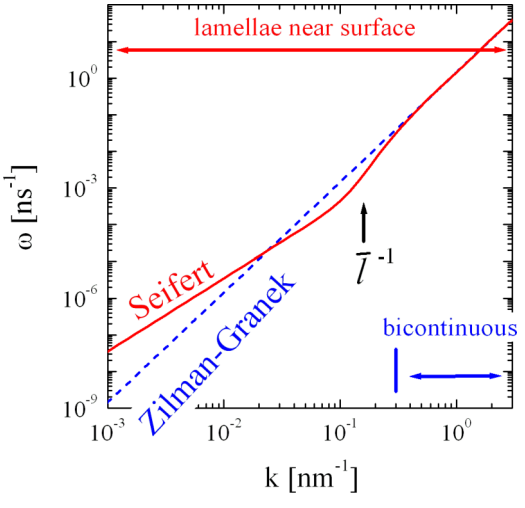

FIG. 5. (Color online) Dispersion relation of the Seifert theory compared to the Zilman-Granek theory. The classical Zilman-Granek theory limited the integration k range by the patch size ξ, which is eliminated for the Seifert theory. The additional long-wavelength modes are responsible for effectively faster relaxations of the lamellar structure close to the surface. The membrane-wall distance is denoted by $\bar{l}$.

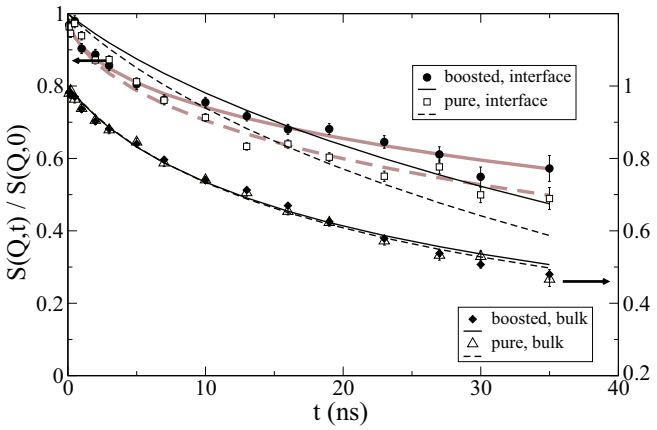

FIG. 6. (Color online) Intermediate scattering function $S(Q,t)$ for the boosted and pure microemulsion at the interface (top curves) and the respective bulk measurements (shifted by -0.2, right axis). The fits are obtained for the Seifert dispersion relation in the Zilman-Granek theory (thin black lines). For the near-surface relaxations, phenomenological fits with a stretching exponent $\beta \approx 0.5$ are included (thick grey lines).

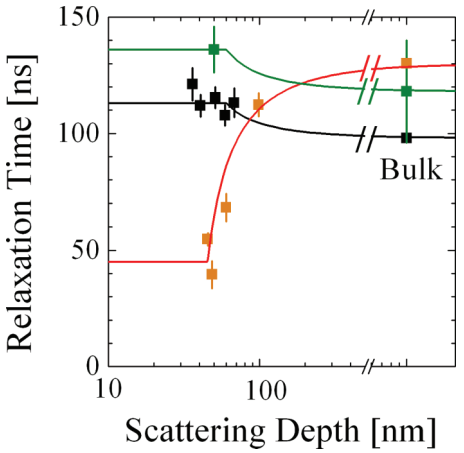

FIG. 7. (Color) Relaxation times for different scattering depths and the bulk microemulsion with polymer (black: measured at J-NSE, green: measured at SNS-NSE) and without polymer (orange: J-NSE) obtained from stretched exponential fits.

of the GISANS peak; so $\xi \approx 10$ nm with no long-range k^2 dependence being observed in this case. The short-range cutoff $k_{\max}$ does not lead to considerable changes to the asymptotic limit of infinitely small surfactant molecules. For pure microemulsions, we measured a value of $\bar{l} = 7.3$ nm [9]. The GINSES experiments [9] revealed a faster decay of the intermediate scattering function $S(Q,t)$ compared to the bulk relaxation. The additional long-wavelength modes introduce further motions to be considered and they are faster compared to the k^3 dependence of the bulk hydrodynamics. The GINSES measurement at a given Q value integrates over a large k-vector range with the emphasis on rather long wavelengths. This is the reason why for pure microemulsions the GINSES relaxation rates are much faster at the surface compared to the bulk.

Figure 6 shows the relaxation in terms of the intermediate scattering function $S(Q,t)$ for a pure microemulsion and one with added diblock copolymers, near the interface and in the bulk. While the bulk measurements show highly similar relaxations for both samples, the pure microemulsion decays faster near the interface than the one with the additive. We described the relaxation curves using the Zilman-Granek theory and applying the Seifert dispersion relation. The intermediate scattering function of this approach reads

$$S(\vec{Q},\tau) \propto \left\langle \int d^2r \int d^2r' \exp[i\vec{Q}_{xy}\cdot(\vec{r}-\vec{r}')] \times \exp\left(-\frac{k_BT}{4\pi^2}Q_z^2 \int_{k_{\min}}^{k_{\max}} \frac{d^2k}{E(k)}[1-e^{i\vec{k}\cdot(\vec{r}-\vec{r}')-\omega(k)\tau}]\right)\right\rangle_\alpha . \quad (3)$$

Details of this formula are given in the Appendix. The brackets $\langle\cdots\rangle_\alpha$ indicate the orientational averaging that is needed for bicontinuous microemulsions. The emphasis was put on larger Fourier times t ($t > 10$ ns), because effectively a different stretching exponent $\beta \sim 0.5$ would be needed at low times, compared to the ideal $\beta = 2/3$ of the Zilman-Granek theory, in order to adequately describe the NSE curves. The more phenomenological approach with a stretched exponential function $S(Q,t) = \exp[-(t/\tau)^\beta]$ is also shown for the near-surface relaxations, which are well described over the whole time range with a smaller β of ca. 0.5. We attribute the variation in β to the proximity to the correlation peak [13,14], where the well-ordered lamellar region introduces subtle variations to the shape of the decay curve due to the DeGennes narrowing, which describes collective motions of neighboring membranes. The general finding of changing stretching exponents β has also been found in Ref. [14], and no suitable theory for the whole Q range was found.

The phenomenological relaxation times τ are depicted in Fig. 7 as a function of the scattering depth Λ. The small error bars and the repetition of the measurement at different sources (with slight uncertainty of the Q calibration) display the reproducibility of the method. The solid lines for the relaxation times $\tau_R(\Lambda)$ in Fig. 7 were obtained from interpolating between two relaxation times τ_{surface} and τ_{bulk} according to

$$\tau_R(\Lambda) = \frac{\tau_{\text{surface}}}{1 + I_{\text{bic}}/I_{\text{lam}}} + \frac{\tau_{\text{bulk}}}{1 + I_{\text{lam}}/I_{\text{bic}}}, \quad (4)$$

with the relative intensities $I_{\text{bic}}/I_{\text{lam}}$ from the GISANS experiments [see Eq. (1)] with the parameters Z and S accordingly. Within the experimental errors, the bulk relaxation times for the pure and polymer-decorated microemulsions are in agreement. The reason for this is the interplay of growing correlation lengths (from about 10 to 13 nm) and increasing bending rigidities (from about 0.9 to 1.15 k_BT) [15]. Therefore, the main focus lies on the near-surface relaxation times. While for the pure microemulsions we observe an acceleration by a factor of 3, the polymer-decorated microemulsion only slightly slows down by about 10%. While the slowing down with respect to the bulk is nearly insignificant, the difference between the pure and polymer-decorated relaxation times is clear and amounts to a factor of about 3. When we described the relaxation curves with the Seifert dispersion relation applied to the Zilman-Granek theory (fits in Fig. 6), we inferred characteristic distances $\bar{l}$ of the first membrane to the wall of 7.8 and 8.1 nm,

assuming a fixed κ of 1.15 (0.9) k_BT for the diblock copolymer containing and the pure microemulsion, respectively (similar to $\bar{l} = 7.3$ nm reported in [9]). Thus the addition of diblock copolymers does not significantly alter this characteristic length. The slowing down of the relaxation with diblock copolymers (increased κ) is a result of higher amplitudes of long-wavelength fluctuations and decreased frequencies ω due to the constraints of more rigid membranes as a fact of the elevated polymer concentration at the rigid surface.

In conclusion, it could be shown with GISANS measurements that amphiphilic diblock copolymers, added as "boosters" to a microemulsion, accumulate at the first and second surfactant membrane layers directly at the interface with a 2–3 times higher polymer concentration than in the bulk microemulsion. They therefore have a very strong influence on surface effects. This is visible in the fluctuation spectrum of the surfactant membrane near the interface, measured with GINSES. It is slowed down significantly. The amplitudes of long-wavelength fluctuations are increased and the frequencies are decreased for the near-surface undulations with the elevated polymer decoration, while the characteristic wall-membrane distance $\bar{l}$ stays mainly unchanged. The study shows how the interaction of a complex liquid with a rigid surface can be modified, which should help to engineer specific properties for nanorheological applications. These findings are relevant for all surfactant-based systems that come in contact with surfaces in typical microemulsion applications such as surface cleaning, where the locally enriched polymers would increase the emulsification abilities, and thus speed up and enlarge the uptake of contaminants.

The research at Oak Ridge National Laboratory's Spallation Neutron Source was sponsored by the Scientific User Facilities Division, Office of Basic Energy Sciences, US Department of Energy.

APPENDIX: INTERMEDIATE SCATTERING FUNCTION OF A MEMBRANE PATCH

Neutron spin-echo spectroscopy measures the intermediate scattering function $S(Q,\tau)$. The dynamic structure factor of a membrane patch as the basic constituent of microemulsions is [20,23]

$$S(\vec{Q},\tau) \propto \left\langle \left| \int_{\text{patch}} d^2r \int_{\text{patch}} d^2r' \exp[i\,\vec{Q}_\parallel \cdot (\vec{r}-\vec{r}')] \times \exp\left\{ i\,Q_z [h(\vec{r},\tau) - h(\vec{r}',0)] \right\} \right| \right\rangle_\alpha . \tag{A1}$$

After statistical averaging over the last exponential factor, one gets

$$S(\vec{Q},\tau) \propto \left\langle \int_{\text{patch}} d^2r \int_{\text{patch}} d^2r' \exp[i\,\vec{Q}_\parallel \cdot\ (\vec{r}-\vec{r}')] \times \exp\left(-\,Q_z^2 \langle [h(\vec{r},\tau) - h(\vec{r}',0)]^2 \rangle \right) \right\rangle_\alpha . \tag{A2}$$

The angular averaging with the angle α is needed for bicontinuous microemulsions with its statistically distributed directions of the surface normal and is omitted for oriented lamellar microemulsions [13–15].

The function $h(\vec{r},\tau)$ describes the membrane displacement from its average position. Expressing the exponent in Eq. (A1) with its Fourier components $h_{\vec{k}}$ with the wave vector $\vec{k}$ of the undulations, we get

$$\langle h_{\vec{k}}(\tau) h_{-\vec{k}}(0) \rangle = \frac{k_BT}{E(k)} \exp[-\omega(k)\tau]. \tag{A3}$$

The dispersion relation for bulk microemulsions is thereby $\omega(k) = \kappa k^3/(4\eta)$, and the reciprocal amplitude $E(k) = \kappa k^4$. After some mathematics one arrives at

$$S(\vec{Q},\tau) \propto \left\langle \int_{\text{patch}} d^2r \int_{\text{patch}} d^2r' \exp[i\,\vec{Q}_\parallel \cdot (\vec{r}-\vec{r}')] \times \exp\left(-\frac{k_BT}{4\pi^2} Q_z^2 \int_{k_{\min}}^{k_{\max}} \frac{d^2k}{E(k)} [1 - e^{i\vec{k}\cdot(\vec{r}-\vec{r}')-\omega(k)\tau}] \right) \right\rangle_\alpha . \tag{A4}$$

A detailed derivation of this formula can be found in Refs. [30,31]. Thermally induced undulations are limited to wave vectors $\vec{k}$ which on the side of large wave vectors are limited by the surfactant molecule size which constitutes the membrane, i.e., $k_{\max} < \pi/a$, because undulations with a wavelength shorter than the surfactant molecule are not possible. On the other hand, the long-wavelength limit (i.e., small-k limit) is of the order of the patch size of a membrane, $k_{\min} > \pi/\xi$. Undulation modes are limited to wavelengths shorter than ξ; the correlation length serves as a cutoff parameter of the undulation mode spectrum for bulk microemulsions. Experiments on bicontinuous microemulsions showed the validity of this assumption of a long-wavelength cutoff [13,15] with $k_{\min} > 1.26 \times \pi/\xi$.

We want to emphasize that the experimental scattering vector Q is not identical to the undulation wave vector k, but just defines the length scale on which one experimentally probes the spectrum of the membrane undulations. The correlation length ξ is a measure of the length scale, on which one can predict the orientation of a membrane.

A membrane close to a flat wall experiences additional contributions to the membrane energy, which have been formulated by Seifert [21,22]. The dispersion relation for small wave vectors k is proportional to k^2 as shown in Fig. 5. We exchanged the dispersion relation in Eq. (A4) with the expression from Seifert [Eqs. (9), (10), and (16) in Ref. [24]], where the distance to the flat wall $\bar{l}$ determines how the undulation mode spectrum is modified:

$$\omega(k,\bar{l},\xi_v) = \Gamma(k,\bar{l}) E(k,\xi_v), \tag{A5}$$

with

$$\Gamma(k,\bar{l}) = \frac{\sinh^2(k\bar{l}) - (k\bar{l})^2}{\sinh^2(k\bar{l}) - (k\bar{l})^2 + \sinh(k\bar{l})\cosh(k\bar{l}) + (k\bar{l})} \frac{1}{2\eta k}, \tag{A6}$$

and

$$E(k,\xi_v) = \kappa\left(k^4 + \xi_v^{-4}\right) + \Sigma k^2. \tag{A7}$$

The surface tension Σ in Eq. (A7) has been set to zero. The ideal correlation length in the Seifert model is $\xi_v = \sqrt{\kappa/k_BT}\ \bar{l}$ [24]. Putting this dispersion relation into Eq. (A4) and fitting the GINSES data with this modified theory allows us to determine $\bar{l}$. The relaxation time is modified

by the changes of the undulation mode spectrum due to the wall-membrane interaction. For membrane patches far away from the membrane, $\bar{l}$ is large and the bulk dispersion relation is recovered (see Fig. 5).

[1] J. Adams, J. Allgaier, and C. Frank, Patent WO 2008132202 (2008).

[2] C. D. Tsakiroglou, C. A. Aggelopoulos, D. N. Tzovolou, M. A. Theodoropoulou, and D. G. Avraam, Int. J. Multiphase Flow **55**, 11 (2013).

[3] V. C. Santanna, F. D. S. Curbelo, T. N. Castro Dantas, A. A. Dantas Neto, H. S. Albuquerque, and A. I. C. Garnica, Journal of Petroleum Science and Engineering **66**, 117 (2009).

[4] C. Cottin-Bizonne, S. Jurine, J. Baudry, J. Crassous, F. Restagno, and E. Charlaix, Eur. Phys. J. E **9**, 47 (2002).

[5] M. P. Lettinga and S. Manneville, Phys. Rev. Lett. **103**, 248302 (2009).

[6] J.-L. Barrat and L. Bocquet, Phys. Rev. Lett. **82**, 4671 (1999).

[7] P. Huber, S. Grüner, C. Schäfer, K. Knorr, and A. V. Kityk, Eur. Phys. J. Special Topics **141**, 101 (2007).

[8] M. Kerscher, P. Busch, S. Mattauch, H. Frielinghaus, D. Richter, M. Belushkin, and G. Gompper, Phys. Rev. E **83**, 030401 (2011).

[9] H. Frielinghaus, M. Kerscher, O. Holderer, M. Monkenbusch, and D. Richter, Phys. Rev. E **85**, 041408 (2012).

[10] H. Frielinghaus, O. Holderer, F. Lipfert, M. Kerscher, S. Mattauch, and D. Richter, EPJ Web of Conferences **33**, 03005 (2012).

[11] B. Jakobs, T. Sottmann, R. Strey, J. Allgaier, L. Willner, and D. Richter, Langmuir **20**, 6707 (1999).

[12] H. Endo, M. Mihailescu, M. Monkenbusch, J. Allgaier, G. Gompper, D. Richter, B. Jakobs, T. Sottmann, R. Strey, and I. Grillo I, J. Chem. Phys. **115**, 580 (2001).

[13] M. Mihailescu, M. Monkenbusch, H. Endo, J. Allgaier, G. Gompper, J. Stellbrink, D. Richter, B. Jakobs, T. Sottmann, and B. Farago, J. Chem. Phys. **115**, 9563 (2001).

[14] M. Mihailescu, M. Monkenbusch, J. Allgaier, H. Frielinghaus, D. Richter, B. Jakobs, and T. Sottmann, Phys. Rev. E **66**, 041504 (2002).

[15] O. Holderer, H. Frielinghaus, D. Byelov, M. Monkenbusch, J. Allgaier, and D. Richter, J. Chem. Phys. **122**, 094908 (2005).

[16] J. Allgaier and H. Frielinghaus, in *Microemulsions* edited by C. Stubenrauch (Wiley, Chichester, 2009).

[17] M. Monkenbusch, R. Schätzler, and D. Richter, Nucl. Instrum. Methods Phys. Res. A **399**, 301 (1997).

[18] O. Holderer, M. Monkenbusch, R. Schätzler, H. Kleines, W. Westerhausen, and D. Richter, Meas. Sci. Technol. **19**, 034022 (2008).

[19] M. Ohl, M. Monkenbusch, N. Arend *et al*., Nucl. Instrum. Methods Phys. Res. A **696**, 85 (2012).

[20] A. G. Zilman and R. Granek, Phys. Rev. Lett. **77**, 4788 (1996).

[21] M. Kraus and U. Seifert, J. Phys. II France **4**, 1117 (1994).

[22] U. Seifert, Phys. Rev. E **49**, 3124 (1994).

[23] A. G. Zilman and R. Granek, Chem. Phys. **284**, 195 (2002).

[24] G. Gompper and D. M. Kroll, Europhys. Lett. **9**, 59 (1989).